Unified linear response function for zonal flows with full finite orbit effects

Unified linear response function for zonal flows with full finite orbit effects

Cite as: Phys. Plasmas **14**, 112512 (2007); https://doi.org/10.1063/1.2805441
Submitted: 13 June 2007 • Accepted: 15 October 2007 • Published Online: 21 November 2007

T. Watari, Y. Hamada, A. Nishizawa, et al.

Unified linear response function for zonal flows with full finite orbit effects

T. Watari, Y. Hamada, A. Nishizawa, and J. Todoroki
National Institute for Fusion Science, Toki, 509-5292, Japan

(Received 13 June 2007; accepted 15 October 2007; published online 21 November 2007)

A new formulation of the linear response function of electrostatic potential to nonlinear drive (due to turbulence) is presented in this paper; zonal flows play important roles in the self-regulation of turbulence and their basic physics are contained in response functions. Two branches of zonal flows [stationary zonal flow and geodesic acoustic mode (GAM)] are known to exist in the low and high frequency ranges. However, they have been analyzed separately using different approximations due the difference in their frequency ranges. This paper visits this problem and gives a unified expression of the response function by taking full account of finite orbit effects. The drift kinetic equation is integrated along particle orbits by expanding them in Fourier series. Thus, a separate handling of passing and trapped particles is facilitated revealing some important aspects of zonal flows: (1) neoclassical poloidal mode coupling due to finite orbit effects, (2) enhancement of the nonuniform potential field due to reduced parallel transport, and (3) the presence of two propagation bands of GAM as the quadratic dispersion relation is solved. © *2007 American Institute of Physics*.
[DOI: 10.1063/1.2805441]

I. INTRODUCTION

The stationary zonal flow and geodesic acoustic mode (GAM) have received much attention in recent research on plasma energy confinement, for they have weak damping and therefore may be excited to a high enough amplitude to regulate turbulence and anomalous transport.[1–21]

The stationary zonal flow is understood as a flow that survives the shielding effect of neoclassical polarization[19,20] and is expected to be the most effective flow in regulation of turbulence. The possible presence of GAM was pointed out by Winsor *et al.*[22] based on the magnetohydrodynamic equation (MHD), followed by several works improving this original theory: (1) kinetic equations were used to facilitate the evaluation of damping,[23,24] (2) the theory of GAM oscillation was extended to helical systems and the behavior of such oscillation was studied in the lower frequency range,[25,26] (3) enhancement of damping was studied taking finite orbital effects into account,[27,28] and (4) an idea of "effective shearing rate" was introduced[18] regarding the mechanism suppressing turbulence. A comprehensive review of zonal flows is given in Ref. 21. Zonal flows gathered more attention as their existence was confirmed in experimental data.[29–38] One of the most fundamental observations is that both kinds of zonal flows are correlated only within a narrow radial domain, of the order of a few Larmor radii;[29,30] this is a virtuous property from the point of view of improving energy confinement time, for large shearing rates are realized with moderate amplitudes of zonal flows. However, the mechanism determining correlation lengths has not been well investigated yet. Of the two zonal flows, GAM is more easily detected in experiments for it is temporally oscillating. It is reported that the experimental GAM frequency is of the order of $\omega_{\mathrm{exp}}=\sqrt{(T_i+T_e)/m_i}$, which is considerably smaller than the MHD description.[3] Some of the experiments include data that suggest that the frequency of GAM oscillation is not always single.[29,30]

Zonal flows are also observed in numerical simulations. In Ref. 3 it is reported that GAM is propagating in the radial direction. Experiments have not yet confirmed this feature, only reporting the small radial coherency length of GAM.

Reflecting on such results in experiments and simulations, we reformulate the electrostatic response function in the zonal flow frequency range, taking variation in particle (parallel) velocity into consideration. This effect has been naturally included in the response function in low frequency range[19,20] (stationary zonal flow) but not in the higher frequency range (GAM).[23–28] In the latter frequency range a so-called "constant velocity approximation" has been used.

We assume the following form for the potential field driven by external charge perturbation $\rho_{\mathrm{ext}}(\omega,k_r)$, as other papers have assumed in the low frequency range:[19,20]

$$\phi_{l=0}(\omega,k_r)=\sum_{l'}R(\omega,k_r)\rho_{\mathrm{ext}}(\omega,k_r)$$

$$=\sum_{l'}\frac{1}{D(\omega,k_r)}\rho_{\mathrm{ext}}(\omega,k_r). \quad (1)$$

Here, $R(\omega,k_r)\equiv 1/D(\omega,k_r)$ is referred to as the response function, and therefore solving for $R(\omega,k_r)$ is identical to solving for $D(\omega,k_r)$. It is expected that the dispersion function $D(\omega,k_r)$ in the denominator approaches a constant value at the low frequency limit giving the so-called neoclassical shielding effect and that $D(\omega,k_r)=0$ is satisfied at a certain frequency ω in the higher frequency range; the former corresponds to stationary zonal flow and the latter corresponds to GAM.

Thus, the present paper focuses on reformulating $R(\omega,k_r)$ [or $D(\omega,k_r)$] with full inclusion of finite orbit effects. In most of the works in the past, parabolic dispersion functions were solved, which is second order in radial wave number k_r:

$$D(\omega,k_r) \propto [a-b(\omega)]k_r^2. \tag{2}$$

Though Eq. (2), gives the local oscillation frequency of GAM, it is not appropriate for discussion of the radial structure of the GAM. Therefore, we will derive a quadratic dispersion function, adding to it the fourth-order term in k_r:

$$D(\omega,k_r) \propto [a-b(\omega)]k_r^2 + c(\omega)k_r^4. \tag{3}$$

This paper is organized as follows. The general formulation of the response function is made in Secs. II A–II D based on the drift kinetic equation; the distribution function is obtained with full orbital effects in Sec. II A, where the constant velocity approximation is eliminated so that separate treatment of passing and trapped particles is facilitated. The expression of density perturbation is obtained for passing particles in Sec. II B by integrating the distribution function. In Sec. II C, the same procedure of calculation is applied to trapped particles and the appropriate formulas are obtained. Other classical terms, which are due to the finite Larmor radius (FLR) effect, are derived in Sec. II D and added to the neoclassical terms.

In Sec. III, the response function is formulated and it is numerically examined applied to a simple tokamak: Charge neutrality is applied in Sec. III A based on the density perturbation obtained in Sec. II to formulate the response function in the most general form. An approximation is applied to parallel dynamics in Sec. III B so that good insights into the physics are maintained in the numerical calculations that follow.

In Secs. III C 1 and III C 2, second-order charges induced by uniform and nonuniform potential fields are calculated and their differences are discussed. It is found there that neoclassical poloidal mode generation (=coupling) is important in zonal flow dynamics. In Sec. III D, the dispersion relation is obtained including fourth-order terms facilitating studies of radial structure in GAM. The presence of two propagating frequency bands is found there. In Sec. III E, properties of the response function in the low frequency range are numerically examined confirming that the obtained formula is a natural extension of "neoclassical polarization" to all frequency ranges. Other supplemental considerations related to the present model and its possible applications are discussed in Sec. IV. Section V is the concluding section, where the major findings in this paper are summarized.

II. FORMULATION

A. Perturbed distribution function with full orbital effects

We start with the drift kinetic equation (DKE) with independent variables in velocity space (w,μ,σ), which are kinetic energy, magnetic moment, and direction of parallel motion, respectively.

$$\frac{\partial f}{\partial t} + (\vec{v}_\parallel + \vec{v}_D)\cdot\nabla f = \sum_l e(ik_\psi\phi_l)[(\vec{v}_\parallel + \vec{v}_D)\cdot\vec{\nabla}]\frac{\partial}{\partial w} \times \exp(ik_\psi\psi + il\theta - i\omega t) + S. \tag{4}$$

Here, f, $\vec{v}_D$, and $\vec{v}_\parallel$ are the distribution function, drift velocity, and parallel velocity of particles, respectively. We adopt a (ψ,θ,ζ) coordinate system for configuration space with θ the poloidal angle, ζ the toroidal angle, and ψ the poloidal magnetic flux; ψ is used as the flux surface label. We consider tokamaks of arbitrary plasma cross section in this paper and therefore all metrics are functions of θ (and ψ), and provided up-down symmetry of the device, they are even in θ. The wave field has been assumed to be electrostatic, characterized by the frequency ω, the radial wave number k_ψ, the poloidal mode number l, and the amplitude of the perturbation ϕ_l, respectively.

S on the right-hand side is the nonlinear drive due to the turbulence, which generally is a function of t, (θ,ζ,ψ), and (w,μ,σ). However, we do not get into the details of this term considering only resultant external charge $\rho_{\text{ext}}(\omega,k_r)$. The two terms on the right-hand side are thus regarded as the external force and the two terms on the left-hand side compose a propagator.

Previous work[23–28] simplified the propagator by assuming that velocities of particles are constant on their paths, which implies that all particles are assumed to be passing. In this paper, we eliminate this approximation and pursue the integration along particle trajectories to obtain the correct perturbed distribution function:

$$\begin{aligned} f &= e\phi_l\int_{-\infty}^{t} dt'\{[\vec{v}_\parallel(t') + \vec{v}_D(t')]\cdot(ik_\psi\vec{\nabla}\psi + il\vec{\nabla}\theta)\}\frac{\partial f_0}{\partial w} \\ &\quad\times\exp[-i\omega t' + ik_\psi\psi(t') + il\theta(t')] \\ &= [e\phi_l]\frac{\partial f}{\partial w}\exp(-i\omega t + ik_\psi\psi + il\theta) \\ &\quad\times\left\{1 + i\omega\int_0^\infty \exp[i\omega(t'') - ik_\psi\Psi(t,t'') - il\Theta(t,t'')]dt''\right\}, \end{aligned} \tag{5}$$

where $[\theta(t'),\psi(t')]$ is the particle orbit with the final condition $[\psi(t),\theta(t)]=(\psi,\theta)$. For simplification, we have introduced notations $\Theta(t,t'')\equiv[\theta(t)-\theta(t-t'')]$ and $\Psi(t,t'')\equiv[\psi(t)-\psi(t-t'')]$,. Since $\Psi(t,t'')$ is simply periodic regardless of whether particles are passing or trapped, we write $\Psi(t,t'')=\tilde{\Psi}(t,t'')$ with wave indicating periodicity of the quantity. However, $\Theta(t,t'')$ requires separate treatment, for it has secular terms for passing particles, which it does not have for trapped particles. We write

$$\Theta(t,t'') \equiv \tilde{\Theta}(t,t'') - \sigma\omega_{b,*}t'', \tag{6}$$

separating the secular term $(-\sigma\omega_{b,*}t'')$ from the periodic term $[\tilde{\Theta}(t,t'')]$. Here, $\omega_{b,*}$ is the frequency of circulation for passing particles and $\omega_{b,*}=0$ for trapped particles. Using simplified notation, we continue the integration by punctuating time t'' and obtain

$$f=[e\phi_l]\frac{\partial f}{\partial w}\left(1+i\omega\frac{1}{1-e^{i\omega T_b}}\int_0^{T_b}\exp\{-i[k_\psi\tilde{\Psi}(t,t'')+il\tilde{\Theta}(t,t'')]\}\exp[i(\omega+\sigma l\omega_{b*})t'']dt''\right). \tag{7}$$

Here, $T_b=\oint g(\theta)/|v_\parallel|d\theta$ and $g(\theta)\equiv\bar{g}\tilde{g}(\theta)\equiv dl/d\theta$ is a kind of metric for the given magnetic configuration. $T_b=T_b(v,\mu)$ is the circulating time for passing particles and the bounce time for trapped particles. $\omega_b=2\pi/T_b$ and $\bar{g}=(1/2\pi)\int_0^{2\pi}g(\theta)d\theta$. The periodic exponential factor in the integrand is expanded in the power series

$$\exp\{-i[k_\psi\tilde{\Psi}(t,t'')+il\tilde{\Theta}(t,t'')]\}=\sum_n\frac{1}{n!}\{-i[k_\psi\tilde{\Psi}(t,t'')+il\tilde{\Theta}(t,t'')]\}^n. \tag{8}$$

If $l\tilde{\Theta}(t,t'')$ is small with respect to $k_\psi\tilde{\Psi}(t,t'')$ as it is reported in experimental papers,[29,30] we may ignore the former and write

$$\approx\sum_{n,m}\frac{1}{n!}(-i)^n\left(\frac{k_\psi I v_T}{\omega_{c,0}}\right)^n x^n\tilde{\Psi}_{n,m}(\sigma,\theta)\exp[im\omega_b(t'')], \tag{9}$$

where $x=v/v_T$, $v=\sqrt{2w/m}$, $v_T=\sqrt{2T/m}$, and $\sigma(=\pm1)$ designates the direction of the parallel motion. The Fourier component $\tilde{\Psi}_{n,m}(\sigma,\theta)$ is defined as follows:

$$\tilde{\Psi}_{n,m}(\sigma,\theta)=\frac{1}{T_b}\int_0^{T_b}[\tilde{\Psi}(t,t')]^n\exp[-im\omega_b(t'')]dt'', \tag{10}$$

with

$$\tilde{\Psi}(t,t')=\left(\frac{\tilde{v}_\parallel(\theta')}{\tilde{\omega}_c(\theta')}-\frac{\tilde{v}_\parallel(\theta)}{\tilde{\omega}_c(\theta)}\right), \tag{11}$$

where $\tilde{v}_\parallel=v_\parallel/v$ and $\tilde{\omega}_c=\omega_c/\omega_{c,0}$.

In deriving the latter, the toroidal momentum conservation, $\psi(\theta)-Iv_\parallel(\theta)/\omega_c(\theta)=P_\zeta$, was used with conventional notation $I=I(\psi)=RB_t$. Equation (7) is divided into two terms,

$$f=f_{\mathrm{I}}+f_{\mathrm{II}}, \tag{12}$$

$$f_{\mathrm{I}}=-\frac{e\phi_l}{T}f_0, \tag{13}$$

and f_{II} is integrated with an aid of Eq. (9):

$$f_{\mathrm{II}}=\frac{e\phi_l}{T}f_0\left[\sum_n(-i)^n\left(\frac{\varepsilon_p^n}{n!}\right)x^n\times\sum_m\tilde{\Psi}_{n,m}(\sigma,\theta)\frac{\omega}{\omega+(\sigma l\omega_{b*}+m\omega_b)}\right]e^{il\theta}$$
$$=\frac{e\phi_l}{T}f_0\left[\sum_n(-i)^n\left(\frac{\varepsilon_p^n}{n!}\right)x^n\sum_m\tilde{\Psi}_{n,m}(\sigma,\theta)\frac{\zeta_{+\sigma l+m}}{\zeta_{+\sigma l+m}+x}\right]e^{il\theta}, \tag{14}$$

where $\varepsilon_p\equiv(k_\psi Iv_T/\omega_{c,0})$ is regarded as the finite orbit effect parameter representing the wavelength with respect to poloidal Larmor radii. Thus, the finite orbit effect (FOE) is essential to zonal flow physics; from this point of view zonal flows are neoclassical phenomena, similar in situation to classical and neoclassical transports. In the last transformation in Eq. (14), we have defined $\zeta_{\sigma l+m}(\omega,\tilde{\mu})\equiv\tilde{\omega}/(\sigma l\tilde{\omega}_{b*}+m\tilde{\omega}_b)$ using normalized quantities, $\tilde{\omega}=\bar{g}\omega/v_T$, $\tilde{\omega}_b(\tilde{\mu})x\equiv\bar{g}\omega_b(\tilde{\mu},w)/v_T$, $\tilde{\omega}_{b*}(\tilde{\mu})x\equiv\bar{g}\omega_{b*}(\tilde{\mu},w)/v_T$, and $\tilde{\mu}=\mu(B_{\max}/w)$. Thus, solving the distribution function f_{II} is reduced to calculation of a set of values for $\tilde{\Psi}_{n,m}^{\mathrm{passing}}(\sigma,\theta)$.

The Fourier integration [Eq. (10)] is performed (for passing particles) taking advantage of the fact that parallel directions of particles (σ) are unchanged. We obtain

$$\tilde{\Psi}_{n,m}^{\mathrm{passing}}(\sigma,\theta)=\sigma^n\sum_{m_1}\tilde{I}_{m_1,m}^{\mathrm{passing}}\cdot C_{n,m_1}(-1)^{n-m_1}\left(\frac{|\tilde{v}_\parallel(\theta)|}{\tilde{\omega}_c(\theta)}\right)^{n-m_1}\times\exp[-i\sigma m\tilde{\omega}_b\tilde{u}(\theta)]. \tag{15}$$

Here,

$$\tilde{I}_{m_1,m}^{\mathrm{passing}}\equiv\frac{1}{\tilde{T}_b}\int_{-\pi}^{\pi}\frac{\tilde{g}d\theta}{|\tilde{v}_\parallel|}\left(\frac{|\tilde{v}_\parallel(\theta)|}{\tilde{\omega}_c(\theta)}\right)^{m_1}\exp[im\tilde{\omega}_b\tilde{u}(\theta)], \tag{16}$$

with $\tilde{u}(\theta)=\int_0^\theta\tilde{g}/|\tilde{v}_\parallel|d\theta$. ($\tilde{I}_{m_1,m}^{\mathrm{passing}}$ are Fourier coefficients with respect to time.) Since integrand in Eq. (16) is even in θ, a symmetry property $\tilde{I}_{m_1,m}^{\mathrm{passing}}=\tilde{I}_{m_1,-m}^{\mathrm{passing}}$ holds and by inspection $\tilde{I}_{m_1,m}^{\mathrm{passing}}=\delta_{m,0}$ for $m_1=0$.

B. Density perturbation and its symmetry

In this paper, we define "density perturbation" as follows, which is different from normal definition by the multiplication factor $[\tilde{g}(\theta)/\tilde{B}(\theta)]$:

$$\delta n_{\mathrm{ind}}=(\tilde{g}/\tilde{B})\int d^3vf_{\mathrm{ind}}. \tag{17}$$

This is justified for the same factor is multiplied to external density perturbations when charge neutrality is used.

The neoclassical density perturbation is obtained by integrating f_{II} over velocity space or by applying the following operator:

$$(\tilde{g}/\tilde{B})\sum_\sigma\frac{2\pi}{m^2}\int\frac{B}{|v_\parallel|}d\mu\int_0^\infty dw\cdot=(\tilde{g}/\tilde{B})\frac{B_0}{B_{\max}}\sum_\sigma L_{\tilde{\mu}}\cdot L_w\cdot\frac{\tilde{B}}{|\tilde{v}_\parallel|}\cdot, \tag{18}$$

where $\tilde{B}=B(\theta)/B_0$, $L_w=(\pi^{-1/2}\int_0^\infty dxx^2\cdot)$, $\tilde{\mu}=B_{\max}(\mu/w)$, $L_{\tilde{\mu}}^{\mathrm{passing}}=(B_0/B_{\max})(\int_0^1d\tilde{\mu}\cdot)$, and $L_{\tilde{\mu}}^{\mathrm{trapped}}=(B_0/B_{\max})\times(\int_1^{B_{\max}/B_{\min}}d\tilde{\mu}\cdot)$.

By introducing spatial Fourier coefficients

$$\alpha_{n,m_1,\sigma m,l'}^{\mathrm{passing}}=\frac{1}{2\pi}\int_0^{2\pi}\frac{\tilde{g}}{|\tilde{v}_\parallel|}\left(\frac{|\tilde{v}_\parallel(\theta)|}{\tilde{\omega}_c(\theta)}\right)^{n-m_1}\times\exp[-il'\theta-i\sigma m\tilde{\omega}_b\tilde{u}(\theta)]e^{-il'\theta}d\theta, \tag{19}$$

we write

$$\tilde{\Psi}^{\text{passing}}_{n,m}(\sigma,\theta)=\sigma^n\sum_{m_1}\tilde{I}^{\text{passing}}_{m_1,m}\cdot C_{n,m_1}(-1)^{n-m_1}\times\sum_{l''}\alpha^{\text{passing}}_{n,m_1,\sigma m,l'}e^{il''\theta}. \tag{20}$$

Since the integrand in Eq. (19) is even in θ, $\alpha^{\text{passing}}_{n,m_1,\sigma m,l'}$ takes real values and have symmetry properties $\alpha^{\text{passing}}_{n,m_1,-\sigma m,-l'}=\alpha^{\text{passing}}_{n,m_1,\sigma m,l'}$.

By substituting Eqs. (15), (16), (19), (20), and (14) into Eq. (17) and using symmetry properties $\alpha^{\text{passing}}_{n,m_1,-\sigma m,-l'}=\alpha^{\text{passing}}_{n,m_1,\sigma m,l'}$, we obtain

$$\begin{aligned}\delta n^{\text{passing}}_{\text{ind}}&=\frac{e\phi_{l'}}{T}L_{\tilde{\mu}}\cdot\sum_n(-i)^n\left(\frac{\varepsilon_p^n}{n!}\right)\times\sum_{l''}\sum_m C_{n,m_1}(-1)^{n-m_1}\tilde{I}_{m_1,m}\alpha^{\text{passing}}_{n-m_1,-m,l''}\\&\times L_w\cdot\sum_{l''}x^n\left(\frac{\zeta_{l'-m}}{\zeta_{l'-m}+x}+(-1)^n\frac{\zeta_{-l'+m}}{\zeta_{-l'+m}+x}\right)e^{i(l'+l'')}\\&=\frac{e\phi_{l'}}{T}\frac{1}{2}L_{\tilde{\mu}}\cdot\sum_n(i)^n\left(\frac{\varepsilon_p^n}{n!}\right)\times\sum_{m,l''}\sum_{m_1}C_{n,m_1}(-1)^{n-m_1}\tilde{I}_{m_1,m}B^{\text{passing}}_{l',-m}\\&\times(\alpha^{\text{passing}}_{n-m_1,-m,l''})e^{i(l'+l'')\theta},\end{aligned} \tag{21}$$

where $B^{\text{passing}}_{n,l',-m}=[-\zeta_{l'-m}Z_{n+2}(\zeta_{l'-m})]$, with the dispersion function $Z_{n+2}(\zeta_{l'-m})$ defined as follows:

$$Z_{n+2}(\zeta_{l'-m})\equiv 2\frac{1}{\sqrt{\pi}}\int_{-\infty}^{\infty}dx x^{n+2}e^{-x^2}\left(\frac{1}{x-\zeta_{l'-m}}\right). \tag{22}$$

C. Density perturbation of trapped particles

A similar procedure is applied to trapped particles in obtaining the distribution function $f^{\text{trapped}}_{\text{II}}$ and density perturbation $\delta n^{\text{trapped}}_{\text{II}}$. However, it is taken into account that trapped particle changes direction as particles pass through their turning points. We find $\tilde{I}^{\text{trapped}}_{m_1,m}$ can be written in a similar form to $\tilde{I}^{\text{passing}}_{m_1,m}$ with a slight modification:

$$\tilde{I}^{\text{trapped}}_{m_1,m}\equiv\frac{1}{\tilde{T}_b}[1+(-1)^{m_1+m}]\int_{-\theta_{\max}}^{\theta_{\max}}\frac{\tilde{g}d\theta}{|\tilde{v}_{\|}|}\left(\frac{\tilde{v}_{\|}(\theta)}{\tilde{\omega}_c(\theta)}\right)^{m_1}\times\exp[im\tilde{\omega}_b\tilde{u}(\theta)]. \tag{23}$$

$\tilde{I}^{\text{trapped}}_{m_1,m}$ takes real values and has the same symmetry properties as $\tilde{I}^{\text{passing}}_{m_1,m}$ does; i.e., $\tilde{I}^{\text{trapped}}_{m_1,m}=\tilde{I}^{\text{trapped}}_{m_1,-m}$. In correspondence to Eq. (19), we define

$$\alpha^{\text{trapped}}_{n,m_1,\sigma m,l'}=\frac{1}{2\pi}\int_{-\pi}^{\pi}\frac{\tilde{g}}{|\tilde{v}_{\|}|}\left(\frac{|\tilde{v}_{\|}(\theta)|}{\tilde{\omega}_c(\theta)}\right)^{n-m_1}\times\exp[-il'\theta-i\sigma m\tilde{\omega}_b\tilde{u}(\theta)]d\theta. \tag{24}$$

The formula $\alpha^{\text{trapped}}_{n,m_1,\sigma m,l'}$ has the same form as that for passing particles, though the integrand should be put zero, where $1-\tilde{\mu}B(\theta)/B_{\max}<0$. By using these expressions, the density perturbation of trapped particles is cast into the same form as that of passing particles:

$$\begin{aligned}\delta n^{\text{trapped}}_{\text{II,ind}}&=\frac{e\phi_{l'}}{T}\frac{1}{2}L_{\tilde{\mu}}\cdot\sum_n(i)^n(\varepsilon_p^n/n!)\times\sum_{m,l''}\sum_{m_1}C_{n,m_1}(-1)^{n-m_1}\tilde{I}^{\text{trapped}}_{n,m}\alpha^{\text{trapped}}_{n-m_1,-m,l''}\\&\times B^{\text{trapped}}_{n,l',-m}\cdot e^{i(l'+l'')\theta}.\end{aligned} \tag{25}$$

Here, $B^{\text{trapped}}_{n,l',-m}=[-\zeta_{-m}Z_{n+2}(\zeta_{-m})]$ is independent of l'; this difference from $B^{\text{passing}}_{n,l',-m}$ is due to the absence of the secular term in Eq. (6).

D. Adiabatic and classical polarization terms

So-called adiabatic density perturbation is obtained by operating $[(\tilde{g}/\tilde{B})L_{\tilde{\mu}}\cdot\Sigma_\sigma L_w\tilde{B}(\theta)/|\tilde{v}_{\|}(\tilde{\mu},\theta)|\cdot]$ to the other part of the perturbed distribution function $f_I=-(en_0\phi_l/T)f_0$. Using an equality $\Sigma_\sigma L_w\cdot f_0=(1/2)n_0$, we obtain

$$\delta n_I^j=-\frac{en_0\phi_l}{T}\sum_{l''}\frac{1}{2}L_{\tilde{\mu}}\cdot\xi^j_{l''}(\tilde{\mu})e^{il''\theta}, \tag{26}$$

where

$$\xi^j_{l''}(\tilde{\mu})=\frac{1}{2\pi}\int_{-\theta_{\max}}^{\theta_{\max}}\frac{\tilde{g}(\theta)}{|\tilde{v}_{\|}|}e^{-il''\theta}d\theta, \tag{27}$$

with superscript j designating the kinds of particle orbit: For passing particles $\theta_{\max}=\pi$ and for trapped particles $\theta_{\max}=\theta_t(\tilde{\mu})$, the poloidal angle at the upper turning point.

Finally, classical polarization terms are added to neoclassical terms δn^j_{II} obtained in subsection B and adiabatic term δn^j_I obtained above; the latter two are obtained from the drift kinetic equation. The classical polarization term is given in the following form in powers of finite Larmor radius (FLR) parameter $\varepsilon_\perp=(k_\perp v_\perp/\omega_c)$:

$$\delta f^j_{\text{classical}}=\frac{e\phi}{T}f_0[J_0^2(\varepsilon_\perp)-1]=\frac{e\phi}{T}f_0\sum_{n=1,2}a_{2n}(\varepsilon_\perp)^{2n}, \tag{28}$$

where $a_2=-1/2$ and $a_4=3/2^5$. $\varepsilon_\perp$ is expressed in terms of FOE parameter ε_p as follows:

$$\varepsilon_\perp^2=\left(\frac{k_\perp v_\perp}{\omega_c}\right)^2=(|R\vec{\nabla}\psi|/I)^2\varepsilon_p^2\frac{1}{\tilde{B}}(B_0\tilde{\mu}/B_{\max}). \tag{29}$$

By operating $(\tilde{g}/\tilde{B})L_{\tilde{\mu}}\cdot\Sigma_\sigma L_w\cdot\tilde{B}(\theta)/|\tilde{v}_{\|}(\tilde{\mu},\theta)|$ to the perturbed distribution function, we obtain

$$\delta n^j_{\text{classical}}(\theta)=\frac{n_0e\phi}{T}L_{\tilde{\mu}}\cdot\sum_{n=1,2}a_{2n}\left(\frac{\varepsilon}{q}\right)^{2n}(\varepsilon_p)^{2n}\tilde{\mu}^n\lambda^{j,2n}_{l''}(\tilde{\mu}), \tag{30}$$

where

$$\lambda_{l''}^{j,n}(\tilde{\mu}) = \frac{1}{2\pi}\int_{-\theta_{\max}}^{+\theta_{\max}} w_n\left(\frac{q}{\varepsilon}\right)^n\left(\frac{\tilde{g}}{|\tilde{v}_\parallel|\tilde{B}^{n-1}}(|R\vec{\nabla}\psi|/I)^n\right)e^{-il''\theta}d\theta \tag{31}$$

with $w_n=\Sigma_\sigma L_w\cdot x^n f_0$; i.e., $w_2=3/4$ and $w_4=15/8$. $(q/\varepsilon)^2$ and $(\varepsilon/q)^2$ are only temporal measures of corresponding quantities as they cancel each other as Eq. (31) is substituted into Eq. (30); q is the safety factor and ε is identified as the inverse aspect ratio r/R in the simple case that we discuss in Sec. III C. Thus, the present formulation is not dependent on the choices of the coordinate system and is applicable to arbitrary magnetic configurations of tokamak, as long as up-down symmetry is provided. All the information about magnetic configuration for confinement are included in metrics $g(\theta)$, $B(\theta)$, and $|R\vec{\nabla}\psi|(\theta)$.

III. RESPONSE FUNCTION AND DISPERSION RELATION

A. Charge neutrality and general formulation

All terms derived in Sec. II are gathered and sum multiplied by $4\pi e_s$ to compose polarization ρ_{ind}:

$$\begin{aligned}\rho_{\text{ind}} = \sum_s k_{D,s}^2 \sum_{j,l''} L_{\tilde{\mu}}^j \cdot \Bigg\{ & -\frac{1}{2}\xi_{l''}^j(\tilde{\mu}) - \frac{1}{2}(\varepsilon/q)^2\varepsilon_p^2\tilde{\mu}\lambda_{l''}^{j,(n=2)}(\tilde{\mu}) \\ & + \frac{3}{2^5}(\varepsilon/q)^4\varepsilon_p^4\tilde{\mu}^2\lambda_{l''}^{j,(n=4)}(\tilde{\mu}) + \frac{1}{2}\sum_n (i)^n(\varepsilon_p^n/n\,!\,) \\ & \times\sum_m \Bigg[\sum_{0\le m_1\le n} C_{n,m_1}\tilde{I}_{n,m_1}^j(-1)^{n-m_1} \\ & \cdot(\alpha_{n-m_1,-m,l''}^j)B_{n,l',-m}^j\Bigg]\Bigg\}\phi_{l'}e^{i(l'+l'')\theta}.\end{aligned} \tag{32}$$

Here, the summation index j denotes two kinds of trajectories: passing $(j=1)$ and trapped $(j=2)$. $k_{\text{D},s}^2=4\pi n_s e_s^2/T_s$ is the Debye wave number, with s denoting the species of plasma: $(s=i)$ and $(s=e)$.

Due to the presence of the multiplying factor 4π, ρ_{ind} is referred to as polarization in the following discussions. We employ hereafter normalizations $\tilde{\rho}=\rho_{\text{ind}}/(k_{\text{D},i}^2\phi_{l=0})$ and $\tilde{\phi}_l=\phi_l/\phi_{l=0}$; by definition $\tilde{\phi}_{l=0}=1$. Expanding $\tilde{\phi}_{l\neq 0}$ and $\tilde{\rho}_l$ in powers of ε_p^n:

$$\tilde{\phi}_l = \sum_n \varepsilon_p^n\tilde{\phi}_l^{(n)} \quad\text{and}\quad \tilde{\rho}_l = \sum_n \varepsilon_p^n\tilde{\rho}_l^{(n)}e^{il\theta}, \tag{33}$$

we obtain the following expression of polarization:

$$\tilde{\rho} = \sum_l \varepsilon_p^n\tilde{\rho}_l^{(n)}e^{il\theta} = \sum_{ns}\sum_{l',n'}(\varepsilon_p^n\tilde{D}_{ns,l',l-l'}\tilde{\phi}_{l'}^{(n-n_s)})e^{il\theta}, \tag{34}$$

i.e.,

$$\tilde{\rho}_l^{(n)} = \sum_{l',0\le ns\le n}(\tilde{D}_{ns,l',l-l'}\tilde{\phi}_{l'}^{(n-ns)}). \tag{35}$$

Here, the operator $\tilde{D}_{ns,l',l-l'}$ is defined as follows:

$$\begin{aligned}\tilde{D}_{ns,l',l-l'} = \sum_s\sum_j (k_{D,s}^2/k_{D,i}^2)L_{\tilde{\mu}}^j\cdot\Bigg[& -\frac{1}{2}\xi_{l-l'}^j(\tilde{\mu})\delta_{ns,0} \\ & + (\varepsilon/q)^{ns}\Bigg(-\frac{1}{2}\tilde{\mu}\lambda_{l-l'}^{j,(n=2)}(\tilde{\mu})\delta_{ns,2} \\ & + \frac{3}{2^5}\tilde{\mu}\lambda_{l-l'}^{j,(n=4)}(\tilde{\mu})\delta_{ns,4}\Bigg) + \frac{1}{2}(i)^{ns}[1/(ns)\,!\,] \\ & \times\sum_m\sum_{0\le m_1\le ns} C_{ns,m_1}(-1)^{ns-m_1}\cdot\tilde{I}_{m_1,m}^j \\ & \times\alpha_{ns,m_1,-m,l-l'}^j B_{ns,l',-m}^j\Bigg].\end{aligned} \tag{36}$$

The subscript s is abbreviated in principle, for electrons contribute only in the lowest order term (which describes parallel dynamics) in FOB parameter ε_p and FLR parameter $(\varepsilon/q)\varepsilon_p$; both are infinitesimally small.

The response function of potential (to external charge) is obtained from charge neutrality

$$\begin{aligned}k_{D,i}^2\phi_{l=0}\sum_n \varepsilon_p^n \sum_{l',ns\le n}(\tilde{D}_{ns,l',l-l'}\tilde{\phi}_{l'}^{(n-ns)})e^{il\theta+ik_\psi\psi} \\ + \rho_{\text{ext},l}(\omega,k_\psi)e^{il\theta+ik_\psi\psi} = 0.\end{aligned} \tag{37}$$

Here, we assume the following form for external charge:

$$\begin{aligned}\rho_{\text{ext}}(\psi,\theta) &= \frac{\tilde{g}(\theta)}{\tilde{B}(\theta)}\sum_s 4\pi e_s n_s(\psi,\theta) \\ &\equiv \sum_l \rho_{\text{ext},l}(\omega,k_\psi)e^{ik_\psi\psi+il\theta},\end{aligned} \tag{38}$$

and study the response of potential to the uniform charge $\rho_{\text{ext}}(\omega,k_\psi)\equiv\rho_{\text{ext},l=0}(\omega,k_\psi)$.

From the $l=0$ component, we obtain

$$k_{\text{D},i}^2\phi_{l=0}\sum_n \varepsilon_p^{(n)}\sum_{l',ns\le n}(\tilde{D}_{ns,l',-l'}\tilde{\phi}_{l'}^{(n-ns)}) + \rho_{\text{ext}}(\omega,k_\psi) = 0, \tag{39}$$

and from the $l\neq 0$ component, we obtain

$$\sum_{l',ns\le n}(\tilde{D}_{ns,l',l-l'}\tilde{\phi}_{l'}^{(n-ns)})e^{il\theta} = 0. \tag{40}$$

This set of linked simultaneous equations may be solved by limiting numbers l and n within some values L and N. The homogeneous equation (40) gives solutions $\tilde{\phi}_{l'\neq 0}^{(n')} = a_{l'}^{n'}(\omega)\tilde{\phi}_{l=0} = a_{l'}^{n'}(\omega)$ and, as they are substituted into Eq. (39), the uniform field relevant to zonal flow is obtained in the following form:

$$\phi_{l=0} = -\frac{\rho_{\text{ext}}}{k_{\text{D},i}^2\sum_n \varepsilon_p^n[\tilde{D}_{n,0,0} + \sum_{1\le ns\le n}\tilde{D}_{ns,l',-l'}a_{l'}^{n-ns}(\tilde{\omega})]}. \tag{41}$$

Thus, we have formally obtained the response function R and dispersion function D in the form of Eq. (1).

B. An approximation in parallel dynamics

In order to keep insights into physics throughout numerical calculation, we look for an appropriate approximation rather than directly solving Eqs. (39) and (40). We write the nth-order equation of Eq. (40) keeping the $ns=0$ term on left-hand side (LHS) and all other terms ($n \geq ns \geq 1$) on right-hand side (RHS):

$$\sum_{l'} \tilde{D}_{ns=0,l',l-l'} \tilde{\phi}_{l'}^{(n)} = -\sum_{l'} \sum_{1 \leq ns \leq n} \tilde{D}_{ns,l',l-l'} \tilde{\phi}_{l'}^{(n-ns)}. \quad (42)$$

The terms on the LHS are subject to the following transformation:

$$\begin{aligned} LHS &= \sum_{j,s} \sum_{l' \neq 0} (k_{D,s}^2/k_{D,i}^2) L_{\tilde{\mu}} \cdot \left\{ -\frac{1}{2} \xi_{l-l'}^{j} \right. \\ &\quad \left. + \frac{1}{2} \sum_{m} I_{0,m} (\alpha_{0,0,-m,l-l'}^{j}) B_{ns,l',-m}^{j} \right\} \tilde{\phi}_{l'}^{(n)} \\ &= -\sum_{s} (k_{D,s}^2/k_{D,i}^2) L_{\tilde{\mu}} \cdot \sum_{l'} \left(\frac{1}{2} \xi_{l-l'}^{j=\text{passing}} \right) (1 + \zeta_{l'} Z_2(\zeta_{l'})) \tilde{\phi}_{l'}^{(n)}, \end{aligned} \quad (43)$$

In the transformation, $m_1 \leq ns = 0$ induced $m_1 = 0$, $m_1 = 0$ induced $I_{m_1,m} = \delta_{m,0}$, and $m = 0$ induced

$$\begin{aligned} \alpha_{n_s - m_1 = 0, -m = 0, l-l'}^{j} &= (1/2\pi) \int_0^{2\pi} (\tilde{g}/|\tilde{\upsilon}_{\parallel}|) e^{-i(l-l'')\theta} d\theta \\ &= \xi_{l-l'}^{j}(\tilde{\mu}). \end{aligned} \quad (44)$$

In the last transformation, we have also used the identity $(1 - B_{ns=0,l',-m}^{j}) = 0$ for trapped particles ($j=2$); thus, trapped particles cannot participate in the screening of charge along magnetic lines of force. A numerical realization of this model is made choosing a simple tokamak case, i.e., the metric $\tilde{g} = qR$, $\tilde{g}(\theta) \to 1$, and $(|R\vec{\nabla}\psi|/I)(q/\varepsilon) \to 1$ in Eqs. (31) and (37). The calculation is made for the safety factor $q=3$ and the inverse aspect ratio $\varepsilon = 0.2$.

Since $\xi_{l-l'}^{\text{passing}}(\tilde{\mu}) \approx \xi_0^{\text{passing}}(\tilde{\mu}) \delta_{l,l'}$ holds for passing particles in lowest order, we adopt the approximation for the LHS of Eq. (42)

$$\text{LHS} = \tilde{D}_{\parallel,l}^{\text{approx}} \tilde{\phi}_{l}^{(n)} e^{il\theta}, \quad (45)$$

where

$$\begin{aligned} \tilde{D}_{\parallel,l}^{\text{approx}} &\equiv -\sum_{s} (k_{D,s}^2/k_{D,i}^2) L_{\tilde{\mu}}^{\text{passing}} \cdot \frac{1}{2} \xi_0^{\text{passing}}(\tilde{\mu}) \\ &\quad \times [1 + \zeta_l Z_2(\zeta_l)] \end{aligned} \quad (46)$$

and

$$\xi_0^{\text{passing}} = \frac{1}{2\pi} \int \tilde{g}/|\upsilon_{\parallel}| d\theta. \quad (47)$$

Thus, the parallel dynamics is represented by the coefficient $\tilde{D}_{\parallel,l}^{\text{approx}}$. Under this approximation, each $\tilde{\phi}_{l' \neq 0}^{(n)}$ term is calculated using the following formula:

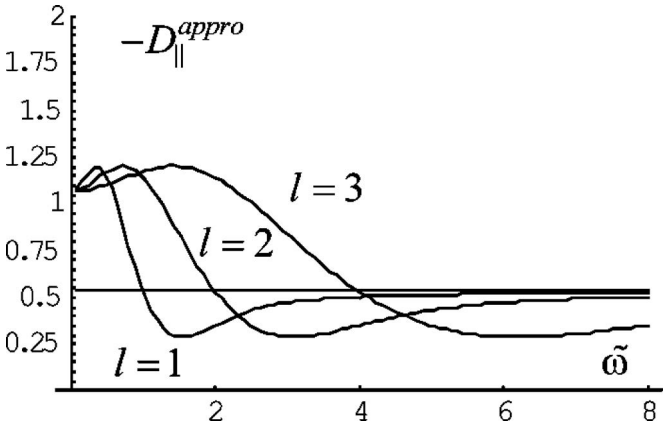

FIG. 1. $\tilde{D}_{\parallel,l}^{\text{approx}}(\omega)$ for various values of l, $|l| \leq 3$: $\tilde{D}_{\parallel}^{\text{approx}}(\omega)$ given by Eq. (54) is plotted vs $\tilde{\omega} = \omega(qR/\upsilon_T)$. It approaches 1.1 and 0.55 in the limits of $\tilde{\omega} \to 0$ and $\tilde{\omega} \to \infty$, respectively. These two values are smaller than 2 and 1 that would be obtained in calculations with constant velocity approximation.

$$\tilde{\phi}_{l \neq 0}^{(n)} = -\frac{\sum_{l'} \sum_{1 \leq ns \leq n} \tilde{D}_{ns,l',l-l'}}{\tilde{D}_{\parallel,l}^{\text{approx}}} \tilde{\phi}_{l'}^{(n-ns)}. \quad (48)$$

Calculations of the coefficients $-\tilde{D}_{\parallel,l}^{\text{approx}}$ are shown in Fig. 1 as function of normalized frequency $\tilde{\omega} = \omega/(\upsilon_{T,i}/qR)$ for several values of poloidal mode numbers l. Electron terms appear only in this term and we have assumed $T_e = T_i$ in this calculation. In Fig. 1, we find that, in the limit of $\omega \to 0$ and $\omega \to \infty$, $-\tilde{D}_{\parallel,l}^{\text{approx}}$ approaches 1.1 and 0.55, respectively, which are smaller than corresponding values 2 and 1, which would be obtained under the constant velocity approximation.[23–28] This is due to the fact that trapped particles cannot participate in parallel dynamics; in drift wave theories $(1 - \sqrt{2\varepsilon})$ is quoted as a factor to indicate this reduction. This factor is substantial in number when the inverse aspect ratio $\varepsilon \approx 0.2$, and frequency dependence incorporated in $-\tilde{D}_{\parallel,l}^{\text{approx}}$ is also important in zonal flow problems.

The RHS of Eq. (42) consists of terms of $\tilde{D}_{ns,l',l-l'}$ with various number $ns \geq 1$: The $\tilde{D}_{ns,l',l-l'}$ is regarded as an ascending operators which, as applied to $\tilde{\phi}_{l'}^{(n-ns)}$, increases its order by ns. Similarly, $\tilde{D}_{ns,l',l-l'}$ is an operator that increases poloidal mode number by $l-l'$. We refer to this process as "neoclassical mode generation" or "neoclassical mode coupling," for it diminishes at the limit of $\varepsilon_p \to 0$.

In order to study the symmetry properties of the potential fields given by Eq. (48), let $\beta(=\pm 1)$ designate the parity of the potential field at order $n-ns$:

$$\tilde{\phi}_{l'}^{n-ns} = (e^{il'\theta} + \beta e^{-il'\theta}) \tilde{\phi}_{|l'|}^{n-ns}. \quad (49)$$

Equation (48) is then rewritten as follows:

$$\tilde{\phi}_l^n e^{il\theta} + \tilde{\phi}_{-l}^n e^{-il\theta} = -\frac{1}{\tilde{D}^{\text{approx}}}\frac{1}{2}(i)^{ns}\left(\frac{1}{ns!}\right) \times \sum_{l'}\sum_{m}\sum_{m_1} C_{ns,m_1}(-1)^{ns-m_1} I^j_{m1,m} \times [e^{il\theta} + (-1)^{ns}\beta e^{-il\theta}]\alpha^j_{ns,m_1,-m,l-l'} \times B_{ns,l',-m}\tilde{\phi}^{n-ns}_{|l'|}. \quad (50)$$

Therefore, with even numbers of ns, the parity of the mode is conserved and with odd numbers of ns, the parity of the mode is reversed. By using this property and starting with the lowest order potential, which is even ($\tilde{\phi}_{l=0}=1$), $\tilde{\phi}_l^{(n)}$ are shown to be even (odd) in θ for even (odd) values of n. Therefore, we only have to calculate $\tilde{\phi}_l^{(n)}$ for $l \geq 0$ in every order of n. Similarly, it is shown that $(i)^n \tilde{\phi}_l^{(n)}/\tilde{\phi}_{l=0}$ are real quantities.

C. Numerical calculations

Since the potential field of each order is obtained using the recurrence formula Eq. (48), we return to Eq. (39) to obtain the response function using the previously unused $l=0$ component. For clarification of the physics, Eq. (39) is divided into two classes of terms, for zero and nonzero l:

$$\tilde{\rho}_l^{(n)} = \tilde{D}_{n,l=0,l=0}\tilde{\phi}_{l=0} + \sum_{ns}\sum_{l'\neq 0}\tilde{D}_{ns,l',l-l'}\tilde{\phi}^{(n-ns)}_{l'}, \quad (51)$$

where $\tilde{\phi}^{(n-ns)}_{l'=0} = \delta_{n,ns}\tilde{\phi}_{l=0}$ is used. The first term is caused by the uniform potential field $\tilde{\phi}_{l=0}$ and the second term consists of various terms resulting from nonuniform fields $\tilde{\phi}^{(n\neq 0)}_{l\neq 0}$.

1. The second-order polarization due to the (zeroth-order) uniform field

Since $\tilde{\rho}^{(n)}_{l=0}=0$ for odd number of n, we need to calculate only the two terms $\tilde{\rho}^{(n=2)}_{l=0}$ and $\tilde{\rho}^{(n=4)}_{l=0}$ to obtain the response function up to fourth order of ε_p, in which we are currently interested. In Fig. 2 are shown polarizations caused by the uniform field: three solid lines show the part contributed by passing particles ($\tilde{\rho}^{(0\to 2)}_{l=0,\text{pas}}$), the part contributed by trapped particles ($\tilde{\rho}^{(0\to 2)}_{l=0,\text{trap}}$), and their sum ($\tilde{\rho}^{(0\to 2)}_{l=0,\text{sum}}$). (Generally, $\tilde{\rho}^{(n_1\to n_2)}_l$ denotes the polarization of order n_2 caused by potential of order n_1.) In order to highlight neoclassical terms, the classical terms are subtracted in this display. The normalized frequency $\tilde{\omega}=\omega/(v_{T,i}/qR)$ is taken for the abscissa. It is noted that $\tilde{\rho}^{(0\to 2)}_{l=0,\text{pas}}$ and $\tilde{\rho}^{(0\to 2)}_{l=0,\text{trap}}$ are comprised of various terms of harmonic interactions ($\tilde{\omega}=m\tilde{\omega}_b$), which occur due to finite orbit effects. A sum over harmonics $-6\leq m\leq 6$ was taken, before being shown in Fig. 2.

A general feature is that the polarizations are positive and small in the high frequency range and negative and large in the low frequency range. The latter range is discussed in Sec. III D in more detail.

The fact that the circulating time of passing particles is shorter than the bounce times of trapped particles suggests to us that trapped particles give dominant effects in low frequency range and passing particles dominate in the high frequency range. This trend is seen in Fig. 2; the contribution of trapped particles to the polarization in GAM frequency range ($\tilde{\omega}\geq 2$) is less than half that of the passing particles, where the population of trapped particles are larger than that of passing particles when $\varepsilon=0.2$.

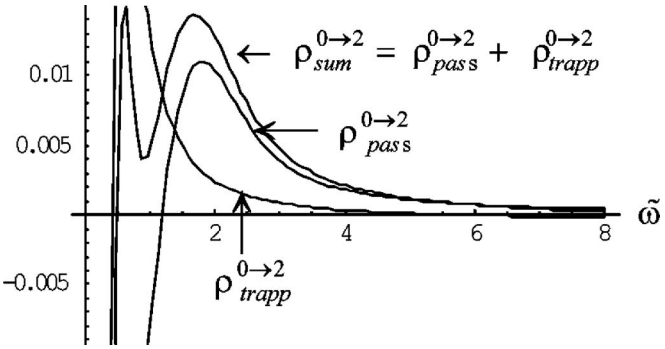

FIG. 2. Second-order polarization $\tilde{\rho}^{(n=2)}_{l=0}$ induced by uniform potential field $\tilde{\phi}_{l=0}$: The polarization is separated into contribution by passing $\tilde{\rho}^{0\to 2}_{l=0,\text{pas}}$ and trapped $\tilde{\rho}^{0\to 2}_{l=0,\text{trap}}$ particles ($\rho^{0\to 2}_{\text{sum}}=\tilde{\rho}^{0\to 2}_{l=0,\text{pas}}+\tilde{\rho}^{0\to 2}_{l=0,\text{trap}}$).

2. The second-order density perturbation due to (first-order) nonuniform field

The nonuniform field $\tilde{\phi}_l^{(1)}$ is created by $\tilde{\phi}^{(0)}_{l=0}$ due to the up-down asymmetry of the density perturbation caused by geodesic curvature as was pointed out in Ref. 26. We write $\tilde{\phi}_l^{(1)}$ separating it into contributions from passing and trapped particles:

$$\tilde{\phi}_l^{(1)} \equiv \tilde{\phi}_l^{(1),\text{pas}} + \tilde{\phi}_l^{(1),\text{trap}}. \quad (52)$$

Figure 3(a) shows $\tilde{\phi}_l^{(1),\text{pas}}$ versus $\tilde{\omega}$ for several values of poloidal mode number l; it is found that $\tilde{\phi}_l^{(1),\text{pas}}$ becomes smaller, in GAM frequency range at higher values of l. However, two modes $\tilde{\phi}^{(1),\text{pas}}_{l=\pm 2}$, and $\tilde{\phi}^{(1),\text{pas}}_{l=\pm 3}$ cannot always be ignored depending on frequency range. Similarly, Fig. 3(b) shows the asymmetric potentials caused by trapped particles, $\tilde{\phi}^{(1),\text{trap}}_{l=\pm 1}$, $\tilde{\phi}^{(1),\text{trap}}_{l=\pm 2}$, and $\tilde{\phi}^{(1),\text{trap}}_{l=\pm 3}$. It is found that trapped particle creates larger $\tilde{\phi}^{(1)}_{l=\pm 1}$ harmonics than passing particles, and $\tilde{\phi}^{(1),\text{trap}}_{l=\pm 2}$ has an amplitude comparable to that of $\tilde{\phi}^{(1),\text{trap}}_{l=\pm 1}$ in the GAM frequency range. This is due to the localized response of the trapped particles to the uniform field $\phi^{(0)}_{l=0}$ localized in the larger major radius board. Given the first-order potential field $\tilde{\phi}_l^{(1)}$, the second-order polarization $\tilde{\rho}^{1\to 2}_l$ is obtained from Eq. (51) taking the $ns=1$ term, of which $\tilde{\rho}^{1\to 2}_{l=0}$ is the other basic component in the zonal flow dynamics. In Fig. 4, $\tilde{\rho}^{1\to 2}_{l=0}$ is shown separated into contributions by passing particles ($\tilde{\rho}^{1\to 2}_{l=0,\text{pas}}$) and trapped particles ($\tilde{\rho}^{1\to 2}_{l=0,\text{trap}}$). We find the contribution of trapped particles is smaller than that of passing particles, similar to the situation that we see in the response of ions to the uniform field. However, there is a notable difference in their mechanisms: for passing particles, the resonant interaction occurs at $\tilde{\omega}=(l'-m)\tilde{\omega}_b$, of which $l'\tilde{\omega}_b$ is due to Doppler shift in the nonuniform field and $-m\tilde{\omega}_b$ is due to the neoclassical harmonic resonance. For trapped particles, only the latter ($\tilde{\omega}=-m\tilde{\omega}_b$) takes place even in response to the nonuniform fields ($l'\neq 0$).

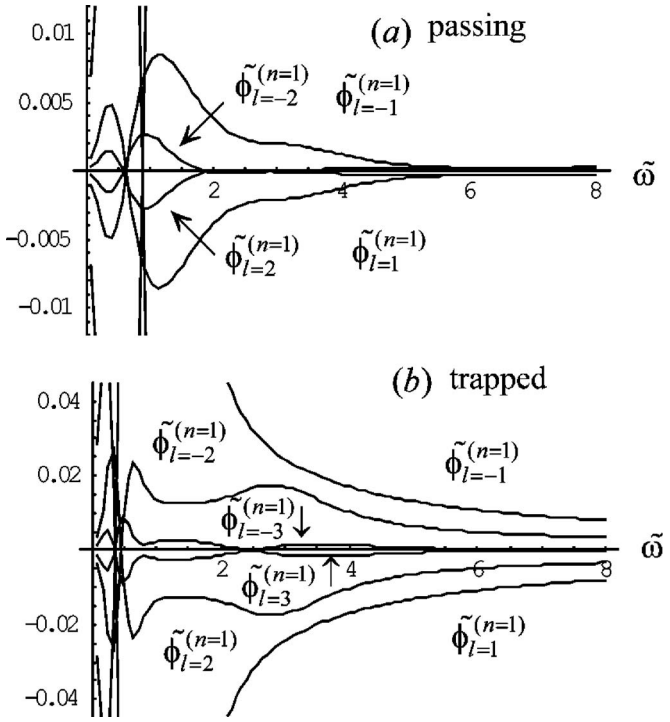

FIG. 3. The first-order nonuniform potential $\phi^{(n=1)}_{l\neq 0}$ generated by zeroth-order uniform field $\phi^{(n=0)}_{l=0}$: $\tilde{\phi}^{(n=1)}_{l\neq 0}$ is plotted vs $\tilde{\omega}$ for several mode number of l: (a) the part contributed by passing particles and (b) the part contributed by trapped particles. The trapped particles give larger contributions than passing particles in generating $\tilde{\phi}^{(1)}_{l}$ for higher poloidal mode number $l>1$. [Imaginary unit $(-i)$ is multiplied by $\tilde{\phi}^{(n=1)}_{l\neq 0}$ on display so that it has real values.]

3. GAM described with parabolic response function

These two $n=2$ terms of polarizations $\tilde{\rho}^{0\to 2}_{l=0}$and $\tilde{\rho}^{1\to 2}_{l=0}$ are gathered to give charge neutrality

$$k^2_{\mathrm{D},i}\varepsilon^2_p(\tilde{\rho}^{0\to 2}_{l=0}+\tilde{\rho}^{1\to 2}_{l=0})\phi^{n=0}_{l=0}+\rho_{\mathrm{ext}}=0, \tag{53}$$

yielding the following parabolic response function and dispersion relation

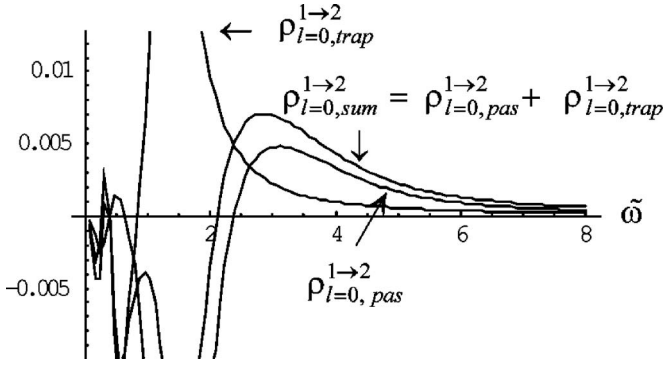

FIG. 4. The second-order density perturbation $\tilde{\rho}^{(n=2)}_{l=0}$ generated by nonuniform first-order potential field $\tilde{\phi}^{(1)}_{l\neq 0}$: The contributions by passing particles $\tilde{\rho}^{1\to 2}_{l=0,\mathrm{pas}}$ and trapped particles $\tilde{\rho}^{1\to 2}_{l=0,\mathrm{trap}}$ are shown together with their sum $\tilde{\rho}^{1\to 2}_{\mathrm{sum}}=\tilde{\rho}^{1\to 2}_{l=0,\mathrm{pas}}+\tilde{\rho}^{1\to 2}_{l=0,\mathrm{trap}}$. Polarizations in this class are predicted to be larger due to the enhancement of nonuniform field, which is attributed to absence of trapped particles in parallel charge screening.

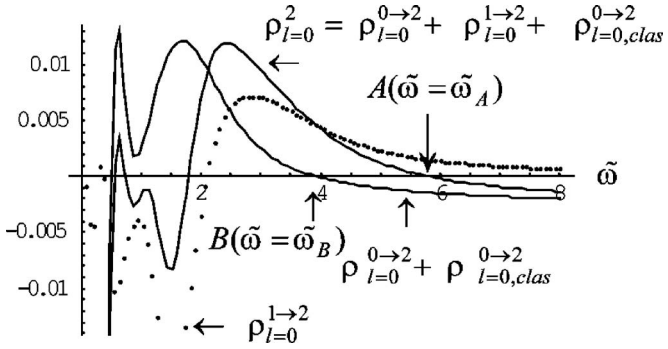

FIG. 5. Determination of GAM frequency with the parabolic dispersion equation: The induced charge $\tilde{\rho}^{(n=2)}_{l=0}=\tilde{\rho}^{0\to 2}_{l=0}+\tilde{\rho}^{1\to 2}_{l=0}+\tilde{\rho}^{0\to 2}_{l=0,\mathrm{clas}}$ is plotted vs $\tilde{\omega}$. $\tilde{\rho}^{0\to 2}_{l=0}$, and $\tilde{\rho}^{1\to 2}_{l=0}$ are the second-order polarizations caused by zeroth- and first-order potentials. The GAM frequency is determined as that where this curve crosses the abscissa; in the figure $(\tilde{\omega}=\tilde{\omega}_A)$ is the solution. In the reference calculation performed without $\tilde{\rho}^{1\to 2}_{l=0}$, the solution is obtained at lower frequency $(\tilde{\omega}=\tilde{\omega}_B)$. Thus, enhanced $\tilde{\rho}^{1\to 2}_{l=0}$ in the present model compensates the reduction in $\tilde{\rho}^{0\to 2}_{l=0}$ and a similar frequency of GAM is predicted to that of conventional theories.

$$\phi^{n=0}_{l=0}=R\rho_{\mathrm{ext}},\quad R=\frac{1}{D}, \tag{54}$$

$$D=k^2_{\mathrm{D},i}\varepsilon^2_p(\tilde{\rho}^{0\to 2}_{l=0}+\tilde{\rho}^{1\to 2}_{l=0})\phi^{n=0}_{l=0}=0. \tag{55}$$

Figure 5 shows the way the frequency of GAM is determined with the parabolic dispersion relation Eq. (55); the sum of the second-order polarizations $\tilde{\rho}^{(2)}_{l=0}=\tilde{\rho}^{(0\to 2)}_{l=0}+\tilde{\rho}^{(1\to 2)}_{l=0}$ is shown in the figure with classical term $\tilde{\rho}^{(0\to 2)}_{l=0,\mathrm{clas}}$ restored. The GAM frequency is determined as $\tilde{\omega}$ where the abscissa is crossed by this curve as indicated with labeled "A" $(\tilde{\omega}=\tilde{\omega}_A)$. Thus, we obtain $\tilde{\omega}_{\mathrm{GAM}}=\tilde{\omega}_A\approx 5.8$, which is interpreted as $\omega_{\mathrm{GAM}}\approx 1.9(v_{T,i}/R)$ when we use the value $q=3$. This value is not much different from those obtained in previous papers.[23–28] Shown in Fig. 5 with a broken line is the polarization due to the nonuniform field $\tilde{\rho}^{(1\to 2)}_{l=0}$. If this part is ignored we obtain the other curve shown by the solid line, which crosses the abscissa at a lower frequency, i.e., $\tilde{\omega}=\tilde{\omega}_B\approx 3.8$, as indicated with the arrow labeled "B," which is interpreted as $\omega_{\mathrm{GAM}}\approx 1.3(v_{T,i}/R)$ with $q=3$. This significant reduction in ω_{GAM} suggests that, in the present model eliminating the constant velocity approximation, the nonuniform potential field is larger than in conventional kinetic models due to the reduction of $-\tilde{D}^{\mathrm{approx}}_{\parallel}$. For this reason, the parabolic response function gives, numerically, a similar frequency to previous theoretical results[23–28] even though trapped particle contribution is small.

D. The fourth-order polarization and quadratic dispersion relation

It is found from Eq. (51) that fourth-order polarization is comprised of four terms, i.e., $\tilde{\rho}^{(n=4)}_{l=0}=\tilde{\rho}^{0\to 4}_{l=0}+\tilde{\rho}^{1\to 4}_{l=0}+\tilde{\rho}^{2\to 4}_{l=0}+\tilde{\rho}^{3\to 4}_{l=0}$, which are caused, respectively, due to uniform field $\tilde{\phi}_{l=0}$ and nonuniform potential fields $\tilde{\phi}^{(1)}_{l\neq 0}$, $\tilde{\phi}^{(2)}_{l\neq 0}$, and $\tilde{\phi}^{(3)}_{l\neq 0}$. As shown in Fig. 6, they have comparable sizes and therefore none of these terms can be ignored. It is noted that their sum $\tilde{\rho}^{n=4}_{l=0}$ changes sign in this calculation at label "C" $(\tilde{\omega}\approx\tilde{\omega}_C\approx 5.5)$; i.e., for $q=3$, $\omega\approx 1.8(v_{T,i}/R)$.

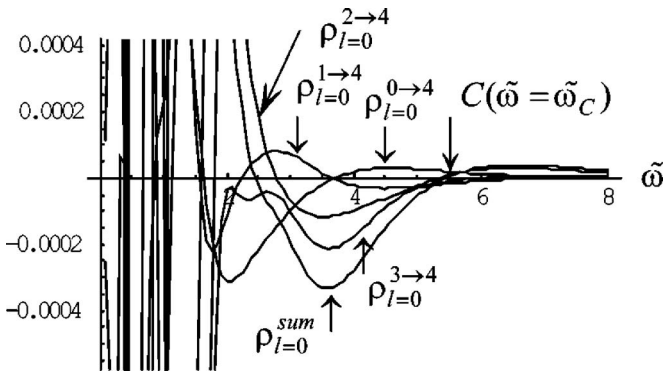

FIG. 6. The fourth-order polarizations $\tilde{\rho}_{l=0}^{0\to4}$, $\tilde{\rho}_{l=0}^{1\to4}$, $\tilde{\rho}_{l=0}^{2\to4}$, $\rho_{l=0}^{3\to4}$, are plotted vs $\tilde{\omega}$: these terms are respectively due to zeroth- through third-order fields $\tilde{\phi}_l^{(0)}$, $\tilde{\phi}_l^{(1)}$, $\tilde{\phi}_l^{(2)}$, and $\tilde{\phi}_l^{(3)}$. The sum of these terms, i.e., $\tilde{\rho}_{l=0}^{n=4,\mathrm{sum}}=\tilde{\rho}_{l=0}^{0\to4}+\tilde{\rho}_{l=0}^{1\to4}+\tilde{\rho}_{l=0}^{2\to4}+\tilde{\rho}_{l=0}^{3\to4}$, crosses the abscissa at label "C" ($\tilde{\omega}=\tilde{\omega}_C$); this frequency is interpreted as resonance frequency, i.e., $\tilde{\omega}=\tilde{\omega}_{\mathrm{resonance}}$, in Fig. 7.

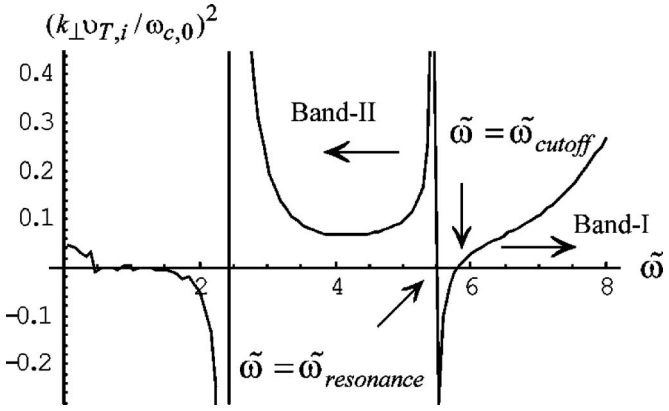

FIG. 7. Dispersion relation of the zonal flow with quadratic dispersion relation: Squared radial wave number $\tilde{k}_\perp^2$ is plotted vs $\tilde{\omega}$; GAM frequency is given as a function of wave number in quadratic dispersion relation revealing its propagating nature. Due to the presence of resonance and cutoff frequencies, i.e., $\tilde{\omega}=\tilde{\omega}_{\mathrm{resonance}}=\tilde{\omega}_C$ and $\tilde{\omega}=\tilde{\omega}_{\mathrm{cutoff}}=\tilde{\omega}_A$, GAM can propagate in two separate frequency bands: Band I and Band II. Considering relation ship of ω with respect to $\upsilon_T[T(\psi)]/qR$, these two bands are translated into two propagation zones in minor radius (ψ).

Adding this fourth-order polarization to second-order equation Eq. (53), we obtain the charge neutrality equation in the following form,

$$k_{D,i}^2[\varepsilon_p^2(\tilde{\rho}_{l=0}^{n=2})\phi_{l=0}^{n=0}+\varepsilon_p^2(\tilde{\rho}_{l=0}^{n=4})\phi_{l=0}^{n=0}]+\rho_{\mathrm{ext}}=0, \tag{56}$$

which gives the fourth-order (or quadratic) response function and dispersion relation

$$\phi_{l=0}=R\rho_{\mathrm{ext}}, \quad R=\frac{1}{D}, \tag{57}$$

$$D=k_{\mathrm{D},i}^2\varepsilon_p^2[(\tilde{\rho}_{l=0}^{n=2})+\varepsilon_p^2(\tilde{\rho}_{l=0}^{n=4})]=0. \tag{58}$$

The expected form Eq. (3) is obtained by writing $a-b(\tilde{\omega})=\tilde{\rho}_{l=0}^{n=2}$ and $c(\omega)=\tilde{\rho}_{l=0}^{n=4}$. Equation (58) gives a solution $\varepsilon_p^2=(Ik_\psi\upsilon_T/\omega_c)^2=-\tilde{\rho}_{l=0}^{n=2}(\omega)/\tilde{\rho}_{l=0}^{n=4}(\omega)$, that is,

$$\tilde{k}_\perp^2=(k_\perp\upsilon_T/\omega_c)^2=-\left(\frac{\varepsilon}{q}\right)^2\frac{\tilde{\rho}_{l=0}^{n=2}(\tilde{\omega})}{\tilde{\rho}_{l=0}^{n=4}(\tilde{\omega})} \tag{59}$$

in terms of new normalization with respect to Larmor radius.

Now the GAM frequency is a function of wave number as shown in Fig. 7. It is found that the GAM has two frequency bands of propagation ($\tilde{k}_\perp^2>0$) for fixed radial position ψ: Band I is above $\tilde{\omega}_A\approx5.8$, where $\tilde{\rho}_{l=0}^{n=2}(\tilde{\omega}_A)=0$ and Band II is below $\tilde{\omega}_C\approx5.5$, where $\tilde{\rho}_{l=0}^{n=4}(\tilde{\omega}_C)=0$. From inspection of Fig. 7, these frequencies are identified as the cutoff and resonance frequencies of GAM: $\tilde{\omega}_{\mathrm{cutoff}}=\tilde{\omega}_A$ and $\tilde{\omega}_{\mathrm{resonance}}=\tilde{\omega}_C$. The frequency conventionally quoted as "GAM frequency" corresponds to the cutoff frequency in terms of the quadratic dispersion relation. Since $\upsilon_T=\upsilon_T[T(\psi)]$, which decreases with increasing minor radius, these two bands in frequency $\tilde{\omega}$ are alternatively interpreted as two propagating zones in ψ. In Band I, the GAM can propagate in the region outside the cutoff layer ($\psi>\psi_A=\psi_{\mathrm{cutoff}}$) for given $\tilde{\omega}$, which is in agreement with the observations in Refs. 3 and 16. Such propagation of GAM waves may be actually taking place both in simulations and experiments. However, some interpretation is needed in relating these two bands to experimentally observed GAM, for the latter is localized in a narrow zone of a few times ion Larmor radius; possible interpretation is that GAM with frequency $\tilde{\omega}$ is condensed and observed at certain positions in minor radius. The cutoff and resonance layers may be candidates to represent Band I and Band II, respectively. A problem in relating cutoff frequency to observed GAM frequency is that wave length generally is long at cutoff layers. In Band II, GAM can propagate inside the resonance layer ($\psi\leq\psi_C=\psi_{\mathrm{resonance}}$). Therefore, the problem that theories predict GAM frequencies higher than experimental ones will be naturally resolved by relating (Band-II) to experimental observations. The general feature that the wavelength is short around resonance points is also a good material in making this correspondence, for GAM is reported to be localized in a thin layer.

(On the contrary, WKB gives the opposite view to the above discussion, for amplitude of waves generally decrease and increase in the vicinity of resonance and cutoff points, respectively. However, the validity of WKB around resonance and cutoff points should be suspect because it should be taken into consideration that all the up-stream excited GAM waves are summed in a statistical manner at resonance layer.)

These bands of propagation depend on the relative position of $\tilde{\psi}_{\mathrm{cutoff}}$ and $\tilde{\psi}_{\mathrm{resonance}}$ layers, topologically. We have seen in Figs. 3(a) and 3(b) that first-order potential has substantial poloidal spectrum spread, due to neoclassical mode coupling; this spectrum spread is amplified in each step of *ns*. The frequency dependence of $\tilde{\rho}_{l=0}^{n=4}(\omega)$ is realized as integrated effects of poloidal spectrum spread in $\tilde{\phi}_l^{(n)}$ and $\tilde{\omega}_{\mathrm{resonance}}(\leftrightarrow\tilde{\psi}_{\mathrm{resonance}})$ is very sensitive to their balance. In Figs. 1 and 5, we have seen that the $\tilde{\omega}_{\mathrm{cutoff}}(\leftrightarrow\tilde{\psi}_{\mathrm{cutoff}})$ is determined by combined effects of parallel and perpendicular dynamics where passing and trapped particles play different roles. Therefore, consideration of full finite orbit effect is important in the GAM frequency range as well as in the lower frequency range. If the GAM propagates transporting

energy as predicted in this analysis, the expected role, an energy reservoir in interplay with turbulence, will require reconsideration.

E. Characteristics of the response function at low frequency

Constant velocity approximation eliminated, the present formulation gives a unified expression of the response function for low frequency stationary zonal flows right through GAM frequency ranges. Its general form has been given in Eqs. (41), (55), or (58). Since we have been looking into the GAM frequency range in the previous sections, figures were out-scaled in the low frequency range. The second-order perturbation $\tilde{\rho}^2_{l=0}=\tilde{\rho}^{0\to 2}_{l=0}+\tilde{\rho}^{1\to 2}_{l=0}$ is shown rescaled in Fig. 8(a), facilitating comprehensive views in all frequency ranges. Apparently, the response of plasma is much larger in the lower frequency range than in the GAM frequency range. The polarization crosses the abscissa twice: the cross at higher frequency corresponds to the ordinary GAM (cutoff) and the cross at lower frequency may give another kind of GAM, though the latter is heavily damped. At the low frequency limit the polarization takes a constant value with negative sign. This form of response is understood as "neoclassical polarization" of low frequency definition; in this paper we have been referring to the induced charge as "polarization" in all frequency ranges. The latter is now understood as generalized "neoclassical polarization," for it is due to finite orbit effects. In Fig. 8(a), $\tilde{\rho}^{1\to 2}_{l=0}$ is shown for reference, manifesting that it diminishes at the limit of $\tilde{\omega}\to 0$. We find thus that the nonuniform fields do not contribute in the neoclassical polarization of narrow definition. In Fig. 8(b), $\tilde{\rho}^{0\to 2}_{l=0}$ is shown decomposed into its parts contributed by passing particles and trapped particles. In Figs. 2 and 5 we have seen that trapped particles gives, in the GAM frequency range, smaller contributions normalized to their populations than passing particles. Contrary, at the limit of $\tilde{\omega}\to 0$, trapped particles give larger contributions than passing particles. In Fig. 8(b), classical polarization is also shown; we find $\tilde{\rho}^{0\to 2}_{l=0,\mathrm{pas}}\to 0.02$, $\tilde{\rho}^{0\to 2}_{l=0,\mathrm{trap}}\to 0.06$, and $\tilde{\rho}^{0\to 2}_{l=0,\mathrm{clas}}\to 0.0022$ at the limit of $\tilde{\omega}\to 0$.

Using these values and parameters in calculation $(q=3,\varepsilon=0.2)$, we obtain

$$\tilde{\rho}^{0\to 2}_{l=0,\mathrm{clas}}+\tilde{\rho}^{0\to 2}_{l=0,\mathrm{trap}}=\tilde{\rho}^{0\to 2}_{l=0,\mathrm{clas}}[1+1.88(q^2/\sqrt{\varepsilon})], \tag{60}$$

which agrees fairly well with the analytical result obtained by Hinton and Rosenbluth in Ref. 19 and 20, where $\tilde{\rho}^{0\to 2}_{l=0,\mathrm{trap}}/\tilde{\rho}^{0\to 2}_{l=0,\mathrm{clas}}=1.6$ is given in place of 1.88. The former value has been confirmed over a rather wide range of ε (see, for example, Ref. 15). This difference becomes smaller at smaller values of ε; we obtain $\tilde{\rho}^{0\to 2}_{l=0,\mathrm{trap}}/\tilde{\rho}^{0\to 2}_{l=0,\mathrm{clas}}\approx 1.73$ for $\varepsilon=0.1$ and $\tilde{\rho}^{0\to 2}_{l=0,\mathrm{trap}}/\tilde{\rho}^{0\to 2}_{l=0,\mathrm{clas}}=1.64$ for $\varepsilon=0.05$, which approaches 1.6 exactly in the limit of $\varepsilon\to 0$. By using Eqs. (16)–(19), (23), (24), and (44) in Eq. (51), we obtain, in fact, exactly the same form as that suggested in Ref. 19 and 20:

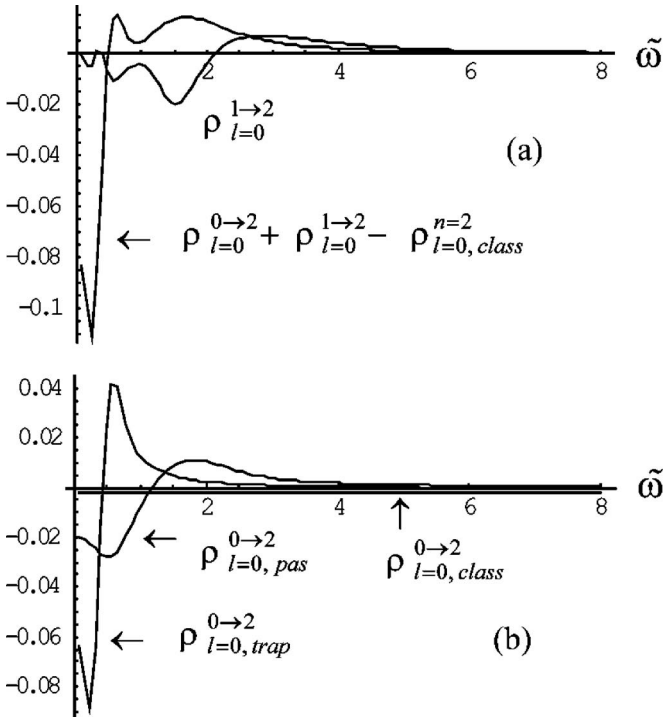

FIG. 8. The second-order polarization in the low frequency range: (a) second-order polarization $\tilde{\rho}^{(n=2)}_{l=0}=(\tilde{\rho}^{(0\to 2)}_{l=0}-\tilde{\rho}^{(0\to 2)}_{l=0,\mathrm{clas}})+\tilde{\rho}^{(1\to 2)}_{l=0}$ is plotted vs $\tilde{\omega}$; the classical part is subtracted in order to see only neoclassical part. The other trace shows $\tilde{\rho}^{(1\to 2)}_{l=0}$ for comparison; this term is found to be small in the limit of $\tilde{\omega}\to 0$. (b) Decomposition of the polarization $\tilde{\rho}^{0\to 2}_{l=0}$ into those carried by passing particles, $\tilde{\rho}^{0\to 2}_{l=0,\mathrm{pas}}$ and trapped particles, $\tilde{\rho}^{0\to 2}_{l=0,\mathrm{trap}}$. Inequality $\tilde{\rho}^{0\to 2}_{l=0,\mathrm{trap}}>\tilde{\rho}^{0\to 2}_{l=0,\mathrm{pas}}$ holds in the limit of $\tilde{\omega}\to 0$; i.e., neoclassical polarization is dominated by trapped particles. The horizontal straight line is $\tilde{\rho}^{0\to 2}_{l=0,\mathrm{clas}}$ in comparison to other terms, where we find that the ratio of neoclassical polarizations to classical polarization is of the order of $q^2/\sqrt{\varepsilon}$.

$$\tilde{\rho}^{(n=2)}_{l=0}=\tilde{D}_{n=2,l=0,l}\tilde{\phi}_{l=0}=-\frac{1}{2\pi\bar{g}}\oint\frac{dl}{\tilde{B}}\int d^3v\left[\left(\frac{\overline{\tilde{v}_{\parallel}(\theta)}}{\tilde{\omega}_c(\theta)}\right)^2-\left(\frac{\overline{\tilde{v}_{\parallel}(\theta)}}{\tilde{\omega}_c(\theta)}\right)^2+\frac{1}{2}\left(\frac{\overline{\tilde{v}_{\perp}(\theta)}}{\tilde{\omega}_c(\theta)}\right)^2\right]. \tag{61}$$

Thus, this response function is an appropriate extension of the R-H response function to higher frequency range including GAM.

IV. DISCUSSION

In this work, we combined DKE by with the well known classical polarization. The classical and neoclassical terms are symmetric in the expression of induced polarization; i.e., up to the fourth order in ε_p, we have

$$\tilde{\rho}_{l=0}=(\varepsilon/q)^2\varepsilon_p^2(\tilde{\rho}^{0\to 2}_{l=0,\mathrm{clas}}+\tilde{\rho}^{0\to 2}_{l=0,\mathrm{neo}})+\varepsilon_p^4(\tilde{\rho}^{0\to 2}_{l=0,\mathrm{clas}}+\tilde{\rho}^{0\to 4}_{l=0,\mathrm{neo}}). \tag{62}$$

The procedure for calculating neoclassical (FOE) terms is analogous to that used in calculating classical (FLR) terms. In calculating neoclassical term, the following "sum-rule" is found to hold with respect to the temporal and spatial Fourier components $\tilde{I}^j_{m_1,m}$ and $\alpha^j_{ns,m_1,-m,l-l'}$:

$$\sum_{m\geq 0}\sum_{0\leq m_1\leq ns} C_{ns,m_1}(-1)^{ns-m_1}\cdot \tilde{I}^j_{m_1,m}\alpha^j_{ns,m_1,-m,l-l'}=0, \quad (63)$$

which, when substituted into Eq. (36), gives the following form:

$$\begin{aligned}\tilde{D}_{ns,l',l-l'} &\propto \sum_{m\geq 0}\sum_{0\leq m_1\leq ns} C_{ns,m_1}(-1)^{ns-m_1}\cdot \tilde{I}^j_{m_1,m} \\ &\quad\times \alpha^j_{ns,m_1,-m,l-l'}B^j_{ns,l',-m} \\ &= \sum_{m>1}\sum_{0\leq m_1\leq ns} C_{ns,m_1}(-1)^{ns-m_1}\cdot \tilde{I}^j_{m_1,m} \\ &\quad\times \alpha^j_{ns,m_1,-m,l-l'}(B^j_{ns,l',-m}-B^j_{ns,l',-m=0}). \quad (64)\end{aligned}$$

Though $\lim_{\tilde{\omega}\to\infty} B^j_{ns,l',-m}\to 0$ does not always hold, $\lim_{\tilde{\omega}\to\infty}(B^j_{ns,l',-m}-B^j_{ns,l',-m=0})\to 0$does hold so that the fundamental requirement that the response of the plasma diminishes in the limit of $\tilde{\omega}\to\infty$ is satisfied. This property was used for numerical accuracy check in the computation.

As a part of this work we are motivated to assess the existing difference between the empirical GAM frequency[29–38] $\omega_{\exp}=\sqrt{(T_i+T_e)/m_i}$ and theoretical predictions: MHD[3,22] and kinetic.[23–28] Theory predictions are $\omega_{\mathrm{MHD}}=\sqrt{2[(5/3)T_i+T_e]/m_i}$ and $\omega_{\mathrm{kinetic}}=\sqrt{2[(7/4)T_i+T_e]/m_i}$, respectively. Assuming that $T_e\sim T_i$, we summarize these results as follows: $\omega_{\exp}\sim v_{T,i}/R$, $\omega_{\mathrm{MHD}}\approx\omega_{\mathrm{kinetic}}$, and $\omega_{\mathrm{theory}}\sim\sqrt{2.7}\omega_{\exp}$.

Notwithstanding that the present model gives a quite different picture for large values of $\varepsilon(\varepsilon\sim 0.2)$, its GAM frequency prediction is not much different from conventional theories in the frame work of parabolic response function. This was discussed in Sec. III C in terms of the creation of nonuniform potential. The quadratic response function explored in the present paper suggests the presence of two bands in GAM, Band I located at higher frequency range than Band II. The GAM frequency discussed above, in this view, is identified as the cutoff frequency, which bounds Band I at low frequency. Similarly, Band II is bound by a resonance frequency (or layer) at high frequency. Thus, the propagation of GAM is characterized by cutoff and resonance pair that may be modeled by a Budden's equation; their distance is considered to affect the GAM dynamics. With a smaller value of $\varepsilon(\varepsilon=0.1)$, the distance between these resonance—and cutoff—layers are further apart than in the case of $(\varepsilon=0.2)$. Thus, Band II is taken as one of the candidates to account for the experimental GAM frequency. The depicted propagating nature of GAM is important in studying the interplay between the drift wave turbulence and zonal flows. For example, a transport barrier, which is characterized by a high temperature gradient, will provide all upstream (small minor radius region) excited GAMs with closely packed resonance layers. Such layers will work as a bank stopping propagation of GAMs; GAMs will dissipate their wave energy there affecting transport.

Finally, a few comments are made regarding the approximations employed in this paper. In order to simplify the calculations, only real part of response function was treated in this paper utilizing only the real part of $Z_{n+2}(\zeta)$. In the intermediate frequency range between GAM and stationary zonal flows, calculations in full complex $\zeta\propto\tilde{\omega}$ plane would be much more informative. We have employed an approximation equation (9) by assuming $l\tilde{\Theta}(t,t'')\ll k_{\psi}\tilde{\Psi}(t,t'')$; this approximation, however, is not essential. If this condition is violated in considering zonal flows of longer radial wavelength, one can calculate the Fourier component of Eq. (8) directly and constitute an algorithm similar to that shown in this paper. The other approximation was used in Eq. (54), with which a small part of mode coupling may be missing. The missing part "mode coupling in parallel dynamics" is retained if the algorithm introduced in Sec. III A is employed and constitute an algorithm leading to Eq. (41).

V. CONCLUSIONS

In this paper, a semi-analytic linear response function is derived for investigations of zonal flows. The method of integrating along particle orbits is adopted without using any approximations and unified expression is obtained valid in all frequency ranges from the stationary zonal flow range to the GAM range. The new formulation includes both zonal flows in the framework of finite orbit effects, and reveals important features in zonal flows which were missing in past works based on constant velocity approximation.

It is found that neoclassical mode coupling is stronger than it was when evaluated with this approximation and generates nonuniform poloidal modes in wider spectrum. Under the separate treatment of passing and trapped particles, it was found that trapped particles do not participate in the relaxation of up-down asymmetry and therefore the excited nonuniform potential field is larger. These enhanced nonuniform fields affect the prediction of GAM frequency in the parabolic dispersion relation.

The present formulation allows writing the dispersion relation to any desired order of finite orbit parameter. The fourth-order term is driven by potentials of various orders spread in various poloidal harmonics. By solving the quadratic dispersion relation it is found that there are two frequency bands in GAM frequency range, which may aid in interpreting the experimentally observed radial structure in GAM. This unified response function is written in rather general form and allows taking into account the geometrical complexity of devices through metrics. Relations between magnetic configuration, zonal flows, and transport improvement may be interesting subjects for future research.

ACKNOWLEDGMENTS

This paper is based on materials used in the presentation at the IAEA ITPA meeting held in Kyoto in 2005. The authors thank Dr. Y. Todo at the NIFS for encouragement of the presentation at the meeting. The authors thank Dr. K. Itoh for valuable discussions in writing this paper. The first author thanks H. Sugama at NIFS for discussing use of the gyrokinetic equation and thanks Dr. T. Shoji at Nagoya University for the kind tutorial of the Mathematica computing program. The authors thank Dr. C. Michael at NIFS for comments and advice in revising this paper.

This work is partly supported by the JSPS-CAS Core University Program.

[1] A. Hasegawa and M. Mima, Phys. Fluids **21**, 87 (1978).
[2] A. Hasegawa and M. Wakatani, Phys. Rev. Lett. **59**,158 (1987).
[3] K. Hallatschek and D. Biskamp, Phys. Rev. Lett. **86**, 1223 (2001).
[4] B. N. Rogers and J. F. Drake, Phys. Rev. Lett. **79**, 229 (1997).
[5] B. N. Rogers, J. F. Drake, and A. Zeiler, Phys. Rev. Lett. **81**, 4396 (1998).
[6] A. M. Dimits, T. J. Williams, J. A. Byers, and B. I. Chohen, Phys. Rev. Lett. **77**, 71 (1996).
[7] B. Scott, Phys. Plasmas **7**, 1845 (2000).
[8] T. S. Hahm, K. H. Burrel, Z. Lin, R. Nazikian, and E. J. Synakovskii, Plasma Phys. Controlled Fusion **42**, A205 (2000).
[9] M. Ramisch, U. Stroth, S. Niedner, and B. Scott, New J. Phys. **5**, 121 (2003).
[10] A. B. Hassam and J. F. Drake, Phys. Fluids B **5**, 4022 (1993).
[11] K. Itoh, K. Hallatschek, and S-I. Itoh, Plasma Phys. Controlled Fusion **47**, 451 (2005).
[12] P. H. Diamond, S. Champeaux, M. Malkov, A. Das, I. Gruzinov, M. N. Rosenbluth, C. Holland, and B. Wecht, Nucl. Fusion **41**, 1067 (2001).
[13] K. Itoh and S-I. Itoh, Plasma Phys. Controlled Fusion **38**, 1 (1996).
[14] S. Satake, M. Okamoto, N. Nakajima, H. Sugama, M. Yokoyama, and C. D. Beidler, Nucl. Fusion **45**, 1362 (2006).
[15] G. Rewoldt, M. A. Beer, M. S. Chance, T. S. Hahm, Z. Lin, and W. M. Tang, Phys. Plasmas **5**, 1815 (1998).
[16] N. Miyato, Y. Kishimoto, and Jiquan Li, Phys. Plasmas **11**, 5557 (2004).
[17] T. S. Hahm, M. A. Beer, Z. Lin, G. W. Hammett, W. W. Lee, and W. M. Tang, Phys. Plasmas **6**, 922 (1999).
[18] T. S. Hahm, Plasma Phys. Controlled Fusion **44**, A87 (2002).
[19] M. N. Rosenbluth and F. L. Hinton, Phys. Rev. Lett. **80**, 724 (1998).
[20] F. L. Hinton and M. N. Rosenbluth, Plasma Phys. Controlled Fusion **41**, A653 (1999).
[21] P. H. Diamond, S-.I. Itoh, K. Itoh, and T. S. Hahm, Plasma Phys. Controlled Fusion **47**, R35 (2005).
[22] N. Winsor, J. L. Johnson, and J. M. Dawson, Phys. Fluids **11**, 2448 (1968).
[23] S. V. Novakovskii, C. S. Liu, R. Z. Sagdeev, and M. N. Rosenbluth, Phys. Plasmas **4**, 4272 (1997).
[24] V. B. Lebedev, P. N. Yushumanov, P. H. Diamond, S. V. Novakovskii, and A. I. Smolyakov, Phys. Plasmas **3**, 3023 (1996).
[25] T. Watari, Y. Hamada, A. Fujisawa, K. Toi, and K. Itoh, Phys. Plasmas **12**, 062304 (2005).
[26] T. Watari, Y. Hamada, T. Notake, N. Takeuchi, and K. Itoh, Phys. Plasmas **13**, 062504 (2004).
[27] H. Sugama, and T. H. Watanabe, Phys. Rev. Lett. **94**, 115001 (2005).
[28] H. Sugama and T. H. Watanabe, Phys. Plasmas **13**, 012501 (2006).
[29] Y. Hamada, A. Nishizawa, T. Ido, T. Watari, M. Kojima, K. Kawasumi, K. Narihara, K. Toi, and JIPP T-IIU Group, Nucl. Fusion **45**, 81 (2005).
[30] A. Fujisawa, K. Itoh, H. Iguchi, K. Matsuoka, S. Okamura, A. Shimizu, T. Minami, Y. Yoshimura, N. Nagaoka, C. Takahashi, M. Kojima, H. Nakano, S. Ohshima, S. Nishimura, M. Isobe, C. Suzuki, T. Akiyama, K. Ida, K. Toi, S-I Ito, and P. H. Diamond, Phys. Rev. Lett. **93**, 165002 (2004).
[31] T. Ido, Y. Miura, K. Kamiya, Y. Hamada, K. Hoshino, A. Fujisawa, K. Itoh, S. I. Itoh, A. Nishizawa, H. Ogawa, Y. Kusama, and JFT-2M group, Plasma Phys. Controlled Fusion **48**, 41 (2006).
[32] G. R. Mackee, R. J. Fonck, M. Jakubowski, K. H. Burrell, K. Hallastschek, R. A. Moyer, W. Nevins, D. L. Rudakov, and X. Xu, Plasma Phys. Controlled Fusion **45**, A477 (2003).
[33] P. M. Schoch, K. A. Conner, D. R. Demers, and X. Zhang, Rev. Sci. Instrum. **74**, 1846 (2003).
[34] Y. W. Tsui, P. M. Schoch, and A. J. Wootton, Phys. Fluids B **5**, 1274 (1993).
[35] M. G. Shats and W. M. Solomon, Phys. Rev. Lett. **88**, 045001 (2002).
[36] G. S. Xu, B. N. Wan, M. Song, and J. Li, Phys. Rev. Lett. **91**, 125001 (2003).
[37] G. D. Conway, B. Scott, J. Schirmer, M. Reich, A. Kendl, and ASDEX Upgrade Team, Plasma Phys. Controlled Fusion **47**, 1165 (2005).
[38] A. V. Melnikov, V. A. Vershkov, L. G. Eliseev, S. A. Grashin, A. V. Gudozhnik, K. I. Krupnik, S. E. Lysenko, V. A. Mavrin, S. V. Perfilov, D. A. Sherukhin, S. V. Soldatov, M. V. Ufimtsev, A. O. Urazbaev, G. Van Oost, and L. G. Zimeleva, Plasma Phys. Controlled Fusion **48**, S87 (2006).